CONSTRUCTION
E-ISSN: 2785-8731
VOLUME 5, ISSUE 2, 2025, 209 - 218
DOI: https://doi.org/10.15282/construction.v5i2.12247

RESEARCH ARTICLE

Development of Global Navigation Satellite System Mission Planning Simulator for Determining Optimum Observation Duration

M.S. Tan, W. A. Wan Aris*, T. A. Musa, A. H. Omar, S.I. Mahadzir, and M. H. Mohd Yatim

Faculty of Built Environment and Surveying, Universiti Teknologi Malaysia, 81210 Johor Bahru, Johor, Malaysia

ABSTRACT - The use of Static Global Navigation Satellite System (GNSS) has become widespread in geodetic applications due to its ability to provide highly accurate positioning. One of the main sources of errors in GNSS positioning is the ionospheric delay, which has a significant impact especially during periods of maximum solar activity. Previous solar cycle 24 indicated that solar maximum and solar minimum occurred in 2014 and 2019, respectively. This highlights the need for extensive collection of GNSS data to minimize the effects of the ionosphere. This study aimed to develop a simulator for mission planning to determine the optimum duration for GNSS static observation. The Malaysia Real-Time Kinematic GNSS network (MyRTKnet) was used, focusing on three baseline categories: short (<50km), medium (50km to 100km), and long (>100km). The static GNSS data were processed using Trimble Business Centre (TBC), and statistical adjustment was performed based on the standard deviation of delta X, delta Y, delta Z, horizontal, and vertical components. The results of the study indicated that to achieve higher precision in GPS baseline solutions during high ionosphere activity, an observation duration of at least two hours is necessary, particularly to improve vertical precision. Furthermore, the precision of the baseline solution was higher during solar maximum compared to solar minimum. A comparison between the simulation and field data acquisition demonstrated that the simulator successfully estimated the horizontal and vertical precision through statistical analysis. Ultimately, it is expected that this simulator will assist surveyors in determining the optimum duration for GNSS static observation.

ARTICLE HISTORY

Received	:	3 April 2025
Revised	:	14 May 2025
Accepted	:	4 August 2025
Published	:	30 December 2025

KEYWORDS

Ionospheric delay
Solar activity
Observation duration
Baseline precision
GNSS simulator

1. INTRODUCTION

The Global Navigation Satellite System (GNSS) is a vital technology that enables positioning within a global reference framework. It supports various applications such as navigation, agriculture, and land surveying [1,2]. However, the required accuracy differs significantly across these applications. A key parameter affecting GNSS accuracy is the Total Electron Content (TEC), which represents the electron density along the path between a satellite and a receiver [3,4]. TEC influences signal propagation, especially during high solar activity when values can exceed 100 Total Electron Content Unit (TECU) in equatorial regions [5]. These effects introduce errors, particularly in carrier-phase measurements [6,7]. To enhance precision, GNSS static observations are employed [8]. This method uses a known reference station and an unknown rover station. Differences between observed and known coordinates allow post-processed differential corrections [9]. Carrier-phase measurements can yield high baseline precision, though factors such as satellite geometry, multipath, and tropospheric effects can impact results [10,11,12,13]. Longer observation durations generally mitigate these effects. Therefore, determining the optimal observation time is crucial for efficient and accurate geodetic work, particularly over long baselines [14,15].

The main sources of GNSS positioning error over long baselines are ionospheric and tropospheric delays. While these can be minimized using double differencing techniques over baselines shorter than 20 km, the method becomes less effective for longer distances [16,17,18]. Since TEC and sunspot activity significantly affect GNSS signal propagation, especially near the equator, determining the optimal observation duration becomes essential for reducing ionospheric effects [19,20]. Longer baselines typically require longer data collection times [21]. This study addresses the need for cost-effective geodetic survey planning by proposing a GNSS simulator that helps determine the optimal observation duration based on baseline length and solar activity. The focus is on short, medium, and long baselines during low and high solar activity periods within Solar Cycle 24.

This research aims to determine the optimum duration for GNSS static observation for three types of baselines which are short-length baseline, medium-length baseline, and long-length baseline including during low and high solar year in Solar Cycle 24. To achieve the aim of the research, there are several objectives that need to be achieved. The objectives include (1) To generate precision of GPS baseline solution during high and low solar year based on different inter-station distance and data observation duration, (2) To estimate the rate of precision of degradation based on result, (3) To develop mission planning simulator for determining optimum duration of GNSS static observation. This paper is divided into four (4) sections. Section one (1) is the introduction which covers the background of study, problem statement, literature

*CORRESPONDING AUTHOR | W. A. Wan Aris | ✉ wananom@utm.my
© 2025 The Author(s). Published by Universiti Malaysia Pahang Al-Sultan Abdullah Press. This is an open access article under the CC BY-NC 4.0 license

review and aim and objectives. Section two (2) is the methodology that covers the three (3) phases. These phases encompass data preparation, data processing, parameter estimation, and the GNSS simulator development. Section three (3) contains the result and analysis fulfilling the three (3) objectives stated in this study. Section four (4) is the study's conclusion and recommendations.

2. LITERATURE REVIEW

GNSS refers to satellite constellations like GPS, GLONASS, Galileo, and BeiDou, which provide users with time and positioning information. These systems operate through three segments: the space segment (satellites), the control segment (ground monitoring stations), and the user segment (receivers). GNSS signals are transmitted through L1 and L2 frequencies, which carry coded and carrier-phase data. While code phase measurements are easier to interpret, carrier-phase measurements provide more precise positioning but are sensitive to errors such as cycle slips [22].

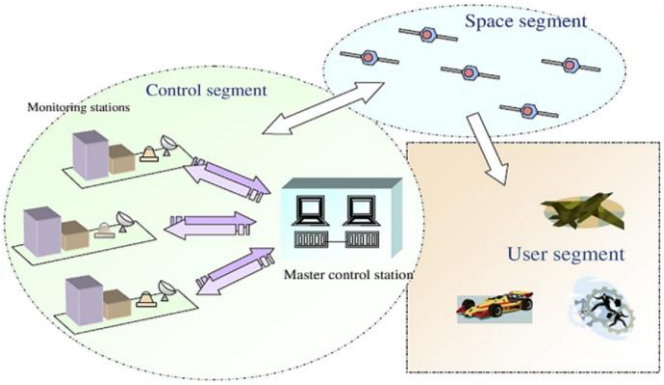

Figure 1. Segments of a satellite navigation system [23]

Several sources contribute to GNSS signal errors, including satellite-dependent, receiver-dependent, and propagation-related factors. Satellite errors include clock and orbit inaccuracies, while receiver errors stem from multipath effects and internal clock mismatches [24,25]. Of particular importance are ionospheric delays, which occur as signals pass through the charged layer of the atmosphere, especially affecting single-frequency receivers [26,27]. TEC plays a critical role in these delays and varies with location, time, and solar activity [28]. The equatorial region, such as Malaysia, often experiences higher TEC due to unique magnetic and atmospheric interactions, with extreme variations during solar maxima and minima [29].

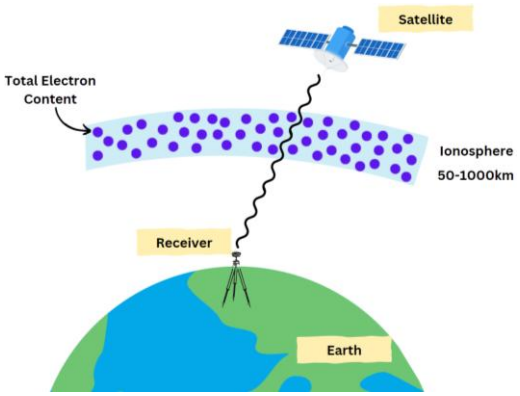

Figure 2. TEC in ionosphere [30,31]

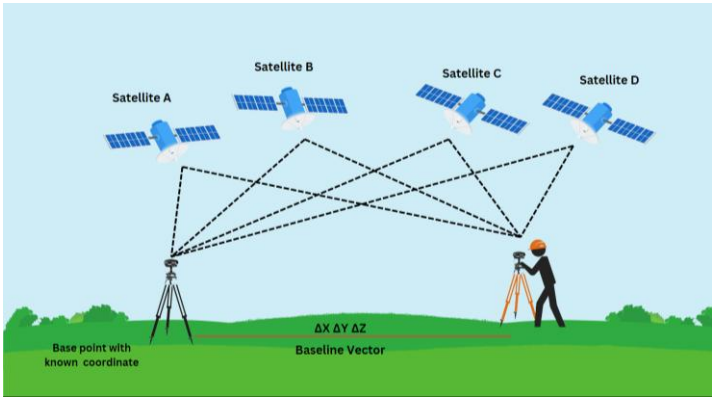

Figure 3. Illustration of baseline vector from GPS static observation [35]

Static GNSS observations, commonly used in high-precision geodetic surveys, involve placing receivers at fixed locations for extended periods. This technique enables accurate 3D coordinate and azimuth calculations without requiring line-of-sight between stations [32,33]. Post-processing differential correction can precisely resolve coordinate differences between a known base and an unknown rover. The baseline vector formed between two stations is estimated using carrier-phase measurements, with double differencing applied to minimize common errors [34]. This approach, often modeled mathematically, enables determination of accurate positions based on observation duration and baseline length.

$$\phi_r^s(t) = \frac{1}{\lambda^s}\rho_r^s(t) + N_r^s + \frac{c}{\lambda^s}\Delta\delta_r^s(t) \quad (1)$$

where,

$\phi_r^s(t)$: Measured carrier phase expressed in cycles between satellite s and receiver r
$\rho_r^s(t)$: Geometric range between satellite s and receiver r
$\Delta\delta_r^s(t)$: Combined receiver and satellite clock bias
N_r^s : Ambiguity Integer number
λ^s : Wavelength
c : Speed of light

During post processing of GPS data, double-differencing technique is applied to reduce the effect of aforementioned GPS errors. Double differencing technique leads to equation 2

$$l_{AB}^{ij} = \alpha_{X_B}^{ij}(t)\Delta X_B + \alpha_{Y_B}^{ij}(t)\Delta Y_B + \alpha_{Z_B}^{ij}(t)\Delta Z_B + \lambda_{L1}N_{AB}^{ij} \quad (2)$$

where,

l_{AB}^{ij} : Linearized equation between satellite i and j to receiver A and B
$\alpha_{X_B}^{ij}$: Arbitrary number for coordinate difference of receiver B
ΔX_B : Coordinate difference of receiver B

Estimation of GPS baseline vector will fix ambiguity parameters (matrix X) requires clean double difference phase data. The following equation $X = (A\hat{}T\ PA)\hat{}(-1)\ (A\hat{}T\ PL)$

The Matrix-vector system can be represented as:

$$\mathrm{X} = \begin{bmatrix} \Delta X_B \\ \Delta Y_B \\ \Delta Z_B \\ N_{AB}^{ij} \\ N_{AB}^{ik} \\ N_{AB}^{im} \end{bmatrix} \quad l = \begin{bmatrix} l_{AB}^{ij}(t_1) \\ l_{AB}^{ik}(t_1) \\ l_{AB}^{im}(t_1) \\ l_{AB}^{ij}(t_2) \\ l_{AB}^{ik}(t_2) \\ l_{AB}^{im}(t_2) \end{bmatrix} \quad \mathrm{A} = \begin{bmatrix} a_{X_B}^{ij}(t_1) & a_{Y_B}^{ij}(t_1) & a_{Z_B}^{ij}(t_1) & \lambda_{L_1} & 0 & 0 \\ a_{X_B}^{ik}(t_1) & a_{Y_B}^{ik}(t_1) & a_{Z_B}^{ik}(t_1) & 0 & \lambda_{L_1} & 0 \\ a_{X_B}^{im}(t_1) & a_{Y_B}^{im}(t_1) & a_{Z_B}^{im}(t_1) & 0 & 0 & \lambda_{L_1} \\ a_{X_B}^{ij}(t_2) & a_{Y_B}^{ij}(t_2) & a_{Z_B}^{ij}(t_2) & \lambda_{L_1} & 0 & 0 \\ a_{X_B}^{ik}(t_2) & a_{Y_B}^{ik}(t_2) & a_{Z_B}^{ik}(t_2) & 0 & \lambda_{L_1} & 0 \\ a_{X_B}^{im}(t_2) & a_{Y_B}^{im}(t_2) & a_{Z_B}^{im}(t_2) & 0 & 0 & \lambda_{L_1} \end{bmatrix}$$

$$P = \begin{bmatrix} \frac{1}{\sigma} & 0 & 0 & 0 & 0 & 0 \\ 0 & \frac{1}{\sigma} & 0 & 0 & 0 & 0 \\ 0 & 0 & \frac{1}{\sigma} & 0 & 0 & 0 \\ 0 & 0 & 0 & \frac{1}{\sigma} & 0 & 0 \\ 0 & 0 & 0 & 0 & \frac{1}{\sigma} & 0 \\ 0 & 0 & 0 & 0 & 0 & \frac{1}{\sigma} \end{bmatrix} \quad (3)$$

X : Baseline Vector with Parameters of Ambiguity
l : Clean Double Differencing
A : Design Matrix
σ : Precision of Double Difference as proposed by remaining errors due to Double Difference Phase Data

Finally, the rover (B) final position can be obtained through 3D Network Adjustment by using Linear Equation below:

$$\begin{bmatrix} X_B \\ Y_B \\ Z_B \end{bmatrix} = \begin{bmatrix} \Delta X_B \\ \Delta Y_B \\ \Delta Z_B \end{bmatrix} + \begin{bmatrix} X_A \\ Y_A \\ Z_A \end{bmatrix} \quad (4)$$

2. METHODOLOGY

Prior to GNSS simulator development a mathematical model needs to be generated. The mathematical model is necessary for explaining variation of baseline vector precision relative to the observation duration based on solar maxima and solar minima. To generate the mathematical model, analytical study on baseline vector precision is required by using GNSS observation data in year 2019 for solar minima and 2014 for solar maxima, respectively. To accomplish the

objectives of the study, the methodology is divided into three phases. These phases encompass data preparation, data processing, parameter estimation, and the GNSS simulator development, as shown in Figure 4.

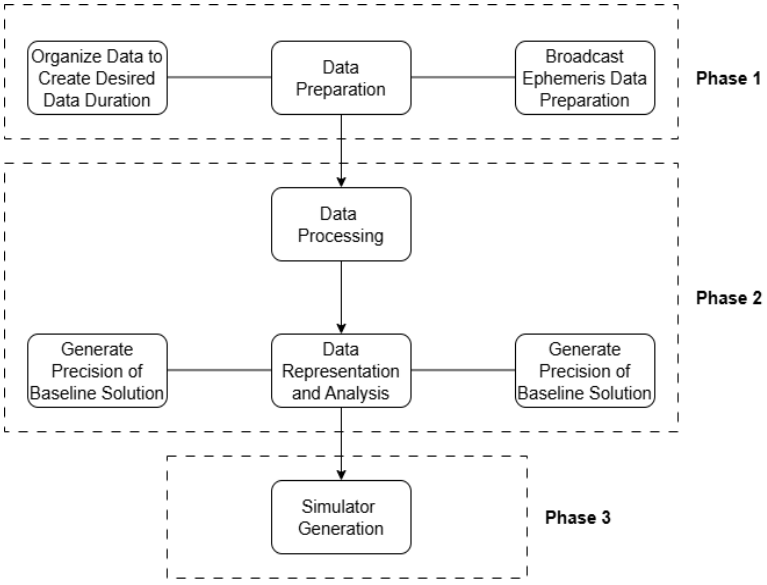

Figure 4. Workflow of the methodology

2.1 Phase 1 Data Preparation

This phase involved preparing GNSS observation data for the study. Data for each station were obtained from the Department of Survey and Mapping Malaysia (JUPEM) in Hatanaka ASCII format, which compresses RINEX files. Broadcast ephemeris data were downloaded through using FileZilla. The data were then organized into different observation durations: 24 hours, 5 hours, 1 hour, 15 minutes, and 5 minutes. GNSS data from the years 2014 (solar maximum) and 2019 (solar minimum) were used, with baseline distances grouped into short, medium, and long categories. The sampling rate for all data was 30 seconds, and the baseline details were listed in Tables 1.

Table 1. Short, medium and long baseline year 2014 and 2019

2014			2019		
From	To	Distance (km)	From	To	Distance (km)
BANT	UPMS	27.769	JHJY	KUKP	44.321
BANT	MERU	37.428	JHJY	TGPG	39.424
BANT	PDIC	44.962	BANT	MERU	37.428
JHJY	TGPG	39.424	BANT	PDIC	44.962
JHJY	KUKP	44.321	BANT	UPMS	27.769
UUMK	SGPT	90.548	BENT	MERU	70.226
UUMK	SIK1	76.223	BENT	SEKI	91.015
USMP	SIK1	68.668	UUMK	SGPT	90.548
JUML	KLAW	87.765	UUMK	SIK1	76.223
BENT	MERU	70.226	JUML	LBIS	93.374
SAND	RANA	160.746	JHJY	JUML	186.932
SAND	SEMP	161.354	KLIP	MRCH	162.484
SAND	MTAW	176.678	KLIP	SETI	165.577
MIRI	BIN1	160.689	KLIP	KUAL	171.021
MIRI	LAB1	170.734	KLIP	AYER	176.113

2.2 Phase 2 Data Processing and Parameter Estimation

Trimble Business Center (TBC) software was used in this phase. All the data including broadcast ephemeris for each day are imported into TBC software. Referring to the table 1, all the base station is assigned with coordinates. All the baseline is process by using single baseline technique and the processing are saved for report generation. Processing report are used to obtain the horizontal precision, vertical precision, Root Mean Square Error (RMSE) and standard deviation. From the report generated by the software, the values of standard deviation for each baseline are then tabulated into Microsoft Excel for equation generation.

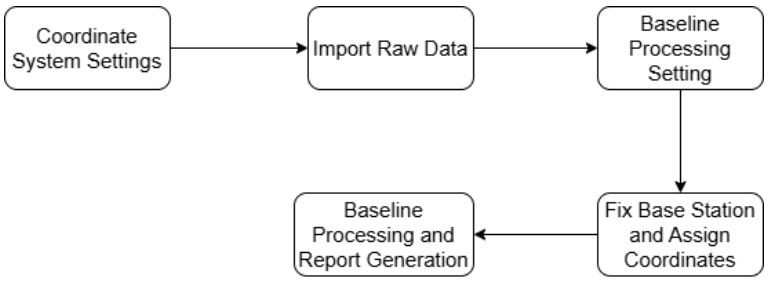

Figure 5. Processing methodology

2.3 Phase 3 GNSS Simulator Development

Trend of baseline vector precision proportional to the GNSS observation duration is generated by categorizing based on solar maxima and minima. In addition, two (2) components of precision is applied such as cartesian X, Y, and Z and horizontal N, E and vertical, h. Equation (5) is an exponential mathematical equation [36].

$$y = Ax\hat{}B \tag{5}$$

where, y is expected baseline precision, and x is observation duration. Two (2) parameters were estimated, and the parameter are used for GNSS simulator development. The simulator is developed by using MATLAB software. It is worth to mention that satellite geometry as explained by Positional Dilution of Precision (PDOP) index (1 to 6) is included in the final optimum duration in order to scale the number of optimal durations. Whereby 1 is best condition meanwhile, 6 is poor satellite geometry. Therefore, the final optimum duration based on user PDOP are calculated by using the formula as shown below.

$$\text{Final Optimum Duration} = \left(\left(\frac{\text{PDOP}}{7} \right) \times x \right) + \text{x} \tag{6}$$

where,

x = initial optimum duration as driven by Equation 5

The performance of the GNSS simulator is conducted by comparing the expected baseline precision from GNSS simulator and the actual baseline precision from GNSS observation. Both baseline precision was based on the amount of GNSS duration as expected by the simulator. From the difference, a chi square test is calculated as shown in Equation 3.3, where Oi is actual precision value meanwhile, Ei is expected precision value.

$$X^2 = \sum \frac{(O_i - E_i)^2}{E_i} \tag{7}$$

where,

X^2 : Chi-Square
O_i : Observed Value
E_i : Expected Value

3. RESULTS AND DISCUSSION

3.1 Trend of Baseline Vector Precision

Figure 5 and 6 show the trend of baseline vector precision proportional to the GNSS observation duration. The graph is generated by based on solar maxima and minima in component ΔX, ΔY, ΔZ, ΔN, ΔE, and Δh. The precision is indicated by standard deviation of the baseline solution. The results show that the standard deviation is lower when longer observation time is utilized. This is because longer observation time provides redundancy of GNSS observation data. This enables effective double differencing technique to minimize GNSS propagation errors.

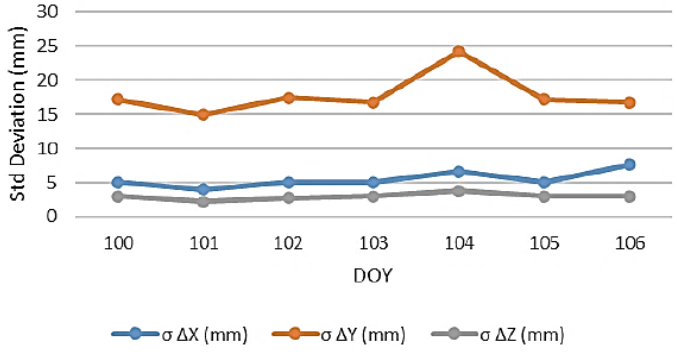

Figure 5. Standard deviation short baseline 2014

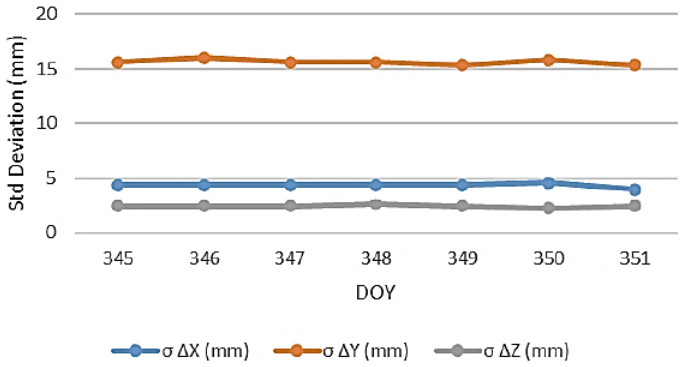

Figure 6. Standard deviation short baseline 2019

Interestingly, both trends during 2014 solar maxima and 2019 solar minima depicted differences in variability. The 2014 data exhibit a substantial spike in the standard deviation of the ΔY parameter around DOY 104. The spike for the ΔY data is quite notable, considering an overall stable situation for the ΔY parameter on other days that were 24 hours for our data collection. The obvious reason for this spike could be due to increases in ionospheric activity during the solar maximum in year 104 that would have imparted sudden and atypical changes in the TEC [37,38]. The conditions in the ionosphere resulted in more variations to reflect as well in the ΔY parameter if measured in certain satellite-receiver geometry or dates where the orbits were grossly aligned as moving in a northern-south direction during that period [39]. By following Equation 5 and Table 2, parameters A and B for each baseline length (short, medium and long) during both events were generated. The trend variability of 2014 as described by the parameter of A and B are larger than the 2019. This is due to the unusual high activities of TEC during solar maxima of 2014. In addition, minor differences are found between data durations of 5 to 24 hours, that can be explained by the better standard deviation. Poor precision is depicted for shorter data durations 15 minutes, and 5 minutes.

Table 2. Parameters of A and B values

Baseline		Solar Maximum		Solar Minimum	
		A	B	A	B
Short	X,Y,Z (mm)	44.694	-0.526	33.477	-0.457
	N,E (mm)	31.488	-0.689	22.365	-0.636
	h (mm)	66.270	-0.410	47.745	-0.344
Medium	X,Y,Z (mm)	40.572	-0.514	29.250	-0.459
	N,E (mm)	26.387	-0.688	18.532	-0.624
	h(mm)	58.855	-0.416	43.766	-0.333
Long	X,Y,Z (mm)	22.270	-0.427	22.531	-0.390
	N,E (mm)	12.152	-0.594	12.188	-0.584
	h (mm)	37.917	-0.331	37.878	-0.304

GNSS Simulator and its Performance

Figure 7 and 8 shows the example of the simulator interface. Depending on the specific objectives of the project, users have the option to simulate precision using either the values of ΔX, ΔY, ΔZ or based on horizontal and vertical precision. The input for this simulator is the year of observation, baseline length and precision needed while the output is the optimum duration. This study utilizes the prediction of solar cycle phase where 2019 to 2022 is consider minimum solar while 2023 to 2026 will utilize the maximum solar equation based on baseline processing result. Table 3 and table 4 tabulates differences of baseline precision in horizontal and vertical components, between GNSS simulator and actual observation. The actual observation was taken in year 2023 which reaching phase of solar maxima in 11 solar cycles. The expected values for horizontal precision and vertical precision are 37.05mm and 74.1mm respectively. The value of Chi-Square tests shows that 0.551mm for horizontal and 58.524mm for vertical, respectively, which are lower than the expected value. This indicates that the GNSS simulator is pass to be used in estimating optimum duration of observation.

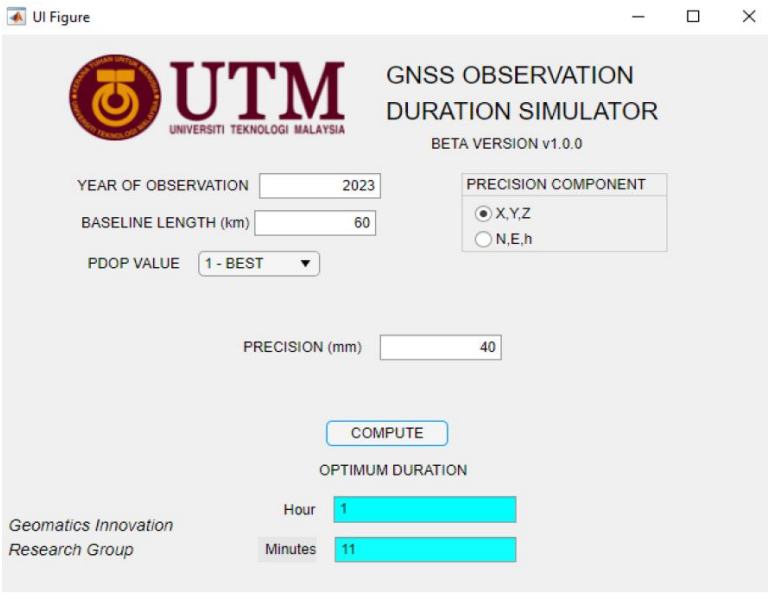

Figure 7. Simulator interface using cartesian precision components (X, Y, Z)

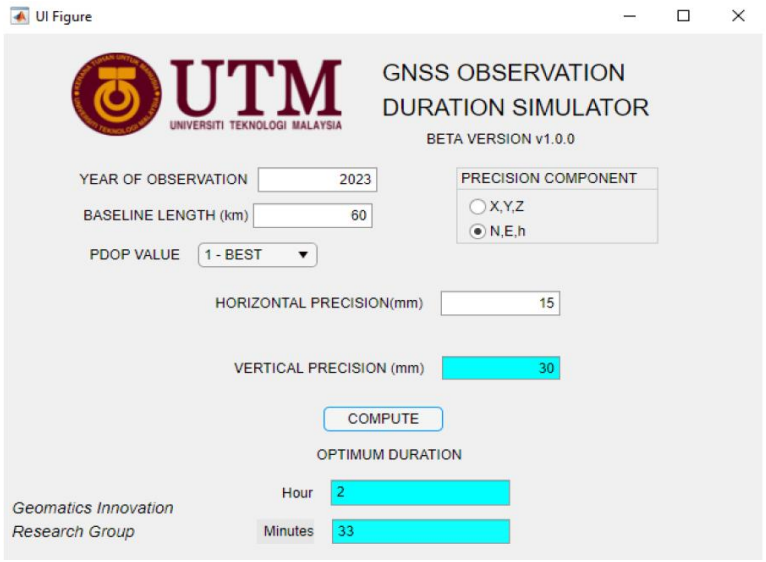

Figure 8. Simulator interface using geodetic precision components (North, East, Height)

Table 3. Differences of baseline precision in vertical component year 2023 (reaching phase of solar maxima in 11 solar cycle)

	GNSS Simulator		Actual GNSS observation		
Baseline Length	Duration (hour & minute)	Expected Precision ($\boldsymbol{E_i}$)	Duration (hour & minute)	Observation Precision (Vertical) ($\boldsymbol{O_i}$)	Difference Precision
(3.572km) with PDOP at 2	2 h 45 m	13.84mm	2 h 45 m	23mm	9.16mm
(44.918km) with PDOP at 2	2 h 46 m	13.80mm	2 h 46 m	63mm	49.20mm
(45.32km) with PDOP at 2	2 h 45 m	13.84mm	2 h 45 m	42mm	28.16mm
(45.327km) with PDOP at 2	1 h 53 m	18.60mm	1 h 53 m	46mm	27.40mm
(3.964km) with PDOP at 3	3 h	14.02mm	3 h	31mm	16.98mm
		$\Sigma E_i = 74.1mm$			$X^2 = 58.42mm$

Table 4. Differences of baseline precision in horizontal component year 2023 (reaching phase of solar maxima in 11 solar cycle)

	GNSS Simulator		Actual GNSS observation		
Baseline Length	Duration (hour & minute)	Expected Precision ($\boldsymbol{E_i}$)	Duration (hour & minute)	Observation Precision (Vertical) ($\boldsymbol{O_i}$)	Difference Precision
(3.572km) with PDOP at 2	2 h 45 m	6.92mm	2 h 45 m	4mm	-2.92mm
(44.918km) with PDOP at 2	2 h 46 m	6.90mm	2 h 46 m	10mm	3.1mm
(45.32km) with PDOP at 2	2 h 45 m	6.92mm	2 h 45 m	8mm	1.08mm
(45.327km) with PDOP at 2	1 h 53 m	9.30mm	1 h 53 m	9mm	-0.3mm
(3.964km) with PDOP at 3	3 h	7.01mm	3 h	6mm	-1.01mm
		$\Sigma E_i = 37.05mm$			$X^2 = 0.551mm$

CONCLUSION

The GNSS measurement are prone to errors primarily caused by satellite dependent errors, ionospheric delays, tropospheric delays, and receiver dependent errors. Ensuring cost-effectiveness is essential in geodetic projects thus, making mission planning for GNSS observation data duration is necessary. This study intended to facilitate observers to determine optimal duration for GNSS static observations via GNSS simulator. The study specifically examines short, medium, and long baselines, solar maxima and solar minima within Solar Cycle 24. During the development of the GNSS simulator, a mathematical model was generated based on an analytical study of baseline vector precision during solar minimum and solar maximum. This model explains how the precision of baseline vectors changes with observation duration. The results of this study showed that longer observation times resulting in lower standard deviation. This is because longer durations provide more redundancy in GNSS observation data. This enables effective double differencing technique to minimize GNSS errors propagation.

AUTHOR CONTRIBUTIONS

Tan Mei Sieng: Conceptualization, Methodology, Software, Data curation,Visualization.

Wan Anom Wan Aris: Supervision.

Tajul Ariffin Musa: Validation.

Abdullah Hisam Omar: Reviewing.

Syahril Irfan Mahadzir: Writing- Original draft preparation and Editing.

Muhammad Hafiz Mohd Yatim: Reviewing.

FUNDING

This study was not supported by any grants from funding bodies in the public, private, or not-for-profit sectors.

DATA AVAILABILITY STATEMENT

The data used to support the findings of this study are included within the article.

ACKNOWLEDGEMENT

The authors would like to thank the Department of Surveying and Mapping Malaysia for providing the GPS data for this study. The author also would like to thank Geomatic Innovation Research Group (GnG) for providing technical support for this study.

CONFLICTS OF INTEREST

The authors declare no conflict of interest.

REFERENCES

[1] C. Specht, T. Szot, P. Dąbrowski, and M. Specht, "Testing GNSS receiver accuracy in Samsung Galaxy series mobile phones at a sports stadium," *Measurement Science and Technology*, vol. 31, no. 6, p. 064006, 2020.

[2] S. Jin, Q. Wang, and G. Dardanelli, "A review on multi-GNSS for earth observation and emerging applications," *Remote Sensing*, vol. 14, no. 16, p. 3930, 2022.

[3] H. Haralambous, T. Leontiou, V. Petrou, A. Kumar Singh, M. Charalambides, N. Lithoxopoulos, et al., "Adjusting ccir maps to improve local behaviour of ionospheric models," *Atmosphere*, vol. 12, no. 6, p. 691, 2021.

[4] C. Oikonomou, I. A. Karolos, S. Bitharis, C. Pikridas, and H. Haralambous, "Ionospheric monitoring using a low-cost gnss receiver. *Ninth International Conference on Remote Sensing and Geoinformation of the Environment* (RSCy2023), vol. 12786, pp. 187-194, 2023.

[5] T. Biswas, P. Banerjee, and A. Paul, "Impact of low-latitude ionospheric effects on precise position determination," *Radio Science*, vol. 57, no. 4, pp. 1-11, 2022.

[6] Z. Zhang, N. Wang, A. Liu, Z. Li, A. Li, L. Wang, et al., "Assessing 1-second roti for ionospheric perturbation monitoring using real-time multi-GNSS data in China," *Space Weather*, vol. 23, no. 2, p. e2024SW004187, 2025.

[7] G. Wang, "A methodology for long-term offshore structural health monitoring using stand-alone GNSS: case study in the Gulf of Mexico," *Structural Health Monitoring*, vol. 23, no. 1, pp. 463-478, 2023.

[8] A. R. Groos, T. J. Bertschinger, C. M. Kummer, S. Erlwein, L. Munz, an A. Philipp, "The potential of low-cost uavs and open-source photogrammetry software for high-resolution monitoring of alpine glaciers: A case study from the kanderfirn (Swiss Alps)," *Geosciences*, vol. 9, no. 8, p. 356, 2019.

[9] X. Li, K. Zhang, F. Ma, W. Zhang, Q. Zhang, Y. Qin, et al., "Integrated precise orbit determination of multi-GNSS and large leo constellations," *Remote Sensing*, vol. 11, no. 21, p. 2514, 2019.

[10] H. A. Msaewe, P. A. Psimoulis, C. M. Hancock, G. W. Roberts, and L. Bonenberg, "Monitoring the response of severn suspension bridge in the United Kingdom using multi-GNSS measurements," *Structural Control and Health Monitoring*, vol. 28, no. 11, p. e2830, 2021.

[11] A. Aboutaleb, A. S. El-Wakeel, H. Elghamrawy, and A. Noureldin, "Lidar/RISS/GNSS dynamic integration for land vehicle robust positioning in challenging GNSS environments," *Remote Sensing*, vol. 12, no. 14, p. 2323, 2020.

[12] F. L. S. Braga and W. R. D. Poz, "Effects of tropospheric refraction on precise point positioning in Brazil," *Pesquisas Em Geociências*, vol. 49, no. 2, p. e118014, 2022.

[13] A. K. Ramavath and P. N. Kumar, "Evaluation of best satellite-receiver geometry for improved IRNSS/GPS position accuracy," *International Journal on Recent and Innovation Trends in Computing and Communication*, vol. 11, no. 9S, pp. 330-333, 2023.

[14] J. G. Singla and S. Trivedi, "Examining quality of DGNSS derived positioning in data in urban city- a case study of an urban city in India," *arXiv preprint arXiv:2411.19794*, 2024.

[15] J. Chen, J. Wang, A. Wang, J. Ding, and Y. Zhang, "SHAtropE—a regional gridded ZTD model for china and the surrounding areas," *Remote Sensing*, vol. 12, no. 1, p. 165, 2020.

[16] T. Suzuki, "GNSS odometry: Precise trajectory estimation based on carrier phase cycle slip estimation," *IEEE Robotics and Automation Letters*, vol. 7, no. 3, pp. 7319-7326, 2022.

[17] X Zhang, Y Dang, C Xu, "A new gpt2w model improved by pso-lssvm for GNSS high-precision positioning," *Journal of Sensors*, vol. 2021, no. 1, p. 9990831, 2021.

[18] B. Kundu, D. Panda, N. K. Vissa, and B. Tyagi, "Novel 2019 coronavirus outbreak through the eyes of GNSS signal," *Journal of the Geological Society of India*, vol. 98, no. 1, pp. 83-87, 2019.

[19] F. Mirmohammadian, J. Asgari, S. Verhagen, and A. Amiri-Simkooei, "Multi-GNSS-weighted interpolated tropospheric delay to improve long-baseline RTK positioning," *Sensors*, vol. 22, no. 15, p. 5570, 2022.

[20] A. Bumrungkit, P. Supnithi, S. Saito, and L. M. M. Myint, "A study of equatorial plasma bubble structure using vhf radar and gnss scintillations over the low-latitude regions," *GPS Solutions*, vol. 26, no. 4, p. 148, 2022.

[21] S. S. Beeck, C. N. Mitchell, A. B. O. Jensen, and L. Stenseng, T. Pinto Jayawardena, and D. H. Olesen, "Experimental determination of the ionospheric effects and cycle slip phenomena for Galileo and GPS in the arctic," *Remote Sensing*, vol. 15, no. 24, p. 5685, 2023.

[22] R. Acharya, "Navigation Receiver," in *Understanding Satellite Navigation*, 1st ed. Amsterdam, The Netherlands: Academic Press (Elsevier), pp. 155–215, 2014.

[23] L. Fangneng, L. Yifeng, X. Jiangning, and W. Miao, "Advances in satellite atomic clock technologies for the GNSS," *Measurement Science and Technology*, vol. 35, no. 1, p. 015027, 2023.

[24] A. Farah, "Single-frequency ionospheric-delay correction from Beidou & GPS systems for northern hemisphere," *Artificial Satellites*, vol. 54, no. 1, pp. 1-15, 2019.

[25] A. Farah, "Behavior of broadcast ionospheric-delay models from GPS, Beidou, and Galileo systems," *Artificial Satellites*, vol. 55, no. 2, pp. 61-76, 2020.

[26] M. Moreno, M. Semmling, G. Stienne, M. Hoque, and J. Wickert, "Characterizing ionospheric effects on GNSS reflectometry at grazing angles from space," *Remote Sensing*, vol. 15, no. 20, p. 5049, 2023.

[27] B. K. Choi, D. H. Sohn, and S. J. Lee, "Correlation between ionospheric TEC and the DCB stability of GNSS receivers from 2014 to 2016," *Remote Sensing*, vol. 11, no. 22, p. 2657, 2019.

[28] O. Jimoh, J. Lei, and F. Huang, "Investigation of daytime total electron content enhancements over the Asian-Australian sector observed from the Beidou geostationary satellite during 2016–2018," *Remote Sensing*, 12(20), 3406, 2020.

[29] A. Silwal, S. P. Gautam, P. Poudel, M. Karki, B. Adhikari, N. P. Chapagain, et al., "Global Positioning System observations of ionospheric total electron content variations during the 15th January 2010 and 21st June 2020 solar eclipse," *Radio Science*, vol. 56, no. 5, p. e2020RS007215, 2021.

[30] S. Kiruthiga and S. Mythili, "Prediction of ionospheric TEC during the occurrence of earthquakes in Indonesia using ARMA and CoK models," *Frontiers in Astronomy and Space Sciences*, vol. 11, p. 1415323, 2024.

[31] D. Janos and P. Kuraś, "Evaluation of low-cost GNSS receiver under demanding conditions in RTK network mode," *Sensors*, vol. 21, no. 16, p. 5552, 2021.

[32] T. Gargula, "Adjustment of an integrated geodetic network composed of GNSS vectors and classical terrestrial linear pseudo-observations," *Applied Sciences*, vol. 11, no. 10, p. 4352, 2021.

[33] V. Hamza, B. Stopar, T. Ambrožič, G. Turk, and O. Sterle, "Testing multi-frequency low-cost GNSS receivers for geodetic monitoring purposes," *Sensors*, vol. 20, no. 16, p. 4375, 2020.

[34] B. Hofmann-Wellenhof, H. Lichtenegger, and E. Wasle, "Mathematical models for positioning," in *GNSS – Global Navigation Satellite Systems: GPS, GLONASS, Galileo, and more*, 1st ed. Berlin/Heidelberg, Germany: Springer Science & Business Media, 2007, pp. 161–191.

[35] J. R. Hass, C. E. Heil, M. D. Weir, and P. Bogacki, Thomas' Calculus, 15th ed. Hoboken, NJ, USA: Pearson, Dec. 29, 2022. [Online]. Available: https://www.pearson.com/en-us/subject-catalog/p/thomas-calculus/P200000007103/9780137616077

[36] S. N. Mukasheva, V. I. Kapytin, and A. M. Malimbayev, "Variations of ionospheric parameters over almaty (Kazakhstan) in 1999–2013," *Solar-Terrestrial Physics*, vol. 5, no. 4, pp. 91-96, 2019.

[37] L. Qian and K. Mursula, "Evaluating F10.7 and F30 radio fluxes as long-term solar proxies of energy deposition in the thermosphere," *Annales Geophysicae Discussions*, vol. 43, no. 1, pp. 175–182, 2025.

[38] Y. I. Yermolaev, I. G. Lodkina, A. A. Khokhlachev, M. Y. Yermolaev, M. O. Riazantseva, L. S. Rakhmanova, et al., "Solar wind parameters in rising phase of solar cycle 25: similarities and differences with solar cycles 23 and 24," *Solar-Terrestrial Physics*, vol. 9, no. 4, pp. 55-62, 2023.